10-20-2006

The p14 fusion-associated small transmembrane (FAST) protein effects membrane fusion from a subset of membrane microdomains

Jennifer A. Corcoran

Jayme Salsman

Roberto De Antueno

Ahmed Touhami

Manfred H. Jericho

See next page for additional authors

Recommended Citation

Jennifer A. Corcoran, et. al., (2006) The p14 fusion-associated small transmembrane (FAST) protein effects membrane fusion from a subset of membrane microdomains.Journal of Biological Chemistry281:4231778. DOI: http://doi.org/10.1074/jbc.M602566200

THE JOURNAL OF BIOLOGICAL CHEMISTRY VOL. 281, NO. 42, pp. 31778–31789, October 20, 2006

The p14 Fusion-associated Small Transmembrane (FAST) Protein Effects Membrane Fusion from a Subset of Membrane Microdomains*[S]

Received for publication, March 20, 2006, and in revised form, August 24, 2006 Published, JBC Papers in Press, August 26, 2006, DOI 10.1074/jbc.M602566200

Jennifer A. Corcoran[‡], Jayme Salsman[‡1], Roberto de Antueno[‡], Ahmed Touhami[§], Manfred H. Jericho[§], Eileen K. Clancy[‡2], and Roy Duncan[‡3]

From the Departments of [‡]Microbiology and Immunology and [§]Physics, Dalhousie University, Halifax, Nova Scotia B3H 1X5, Canada

The reovirus fusion-associated small transmembrane (FAST) proteins are a unique family of viral membrane fusion proteins. These nonstructural viral proteins induce efficient cell-cell rather than virus-cell membrane fusion. We analyzed the lipid environment in which the reptilian reovirus p14 FAST protein resides to determine the influence of the cell membrane on the fusion activity of the FAST proteins. Topographical mapping of the surface of fusogenic p14-containing liposomes by atomic force microscopy under aqueous conditions revealed that p14 resides almost exclusively in thickened membrane microdomains. In transfected cells, p14 was found in both Lubrol WX- and Triton X-100-resistant membrane complexes. Cholesterol depletion of donor cell membranes led to preferential disruption of p14 association with Lubrol WX (but not Triton X-100)-resistant membranes and decreased cell-cell fusion activity, both of which were reversed upon subsequent cholesterol repletion. Furthermore, co-patching analysis by fluorescence microscopy indicated that p14 did not co-localize with classical lipid-anchored raft markers. These data suggest that the p14 FAST protein associates with heterogeneous membrane microdomains, a distinct subset of which is defined by cholesterol-dependent Lubrol WX resistance and which may be more relevant to the membrane fusion process.

Biological membrane fusion is dependent on protein catalysts to mediate the lipid rearrangements required for membrane merger (1, 2). The fusion-associated small transmembrane (FAST) proteins are one such family of membrane fusion catalysts (3). The FAST proteins are a unique group of small (95–140 amino acids) integral membrane proteins encoded by the fusogenic reoviruses, an unusual group of non-enveloped viruses that induce syncytium formation (3–6). Three distinct members of the FAST protein family have been described in recent years: the homologous p10 proteins of avian reovirus and Nelson Bay reovirus and the unrelated p14 and p15 proteins of reptilian reovirus and baboon reovirus, respectively (3–5). Unlike the well characterized fusion proteins of enveloped viruses (7), the FAST proteins are nonstructural viral proteins and are therefore not involved in viral entry into cells. Following their expression inside virus-infected or -transfected cells, the FAST proteins traffic through the endoplasmic reticulum-Golgi pathway to assume a bitopic $N_{exoplasmic}/C_{cytoplasmic}$ topology in the plasma membrane, where they mediate fusion of virus-infected cells to neighboring uninfected cells (8–10). Therefore, the FAST proteins function more as "cellular" rather than viral fusion proteins, mediating cell-cell rather than virus-cell membrane fusion. Furthermore, a recent study using the purified p14 FAST protein of reptilian reovirus reconstituted into artificial lipid bilayers indicated that the FAST proteins are both necessary and sufficient to mediate membrane fusion (11).

In addition to their unique role in the viral replication cycle, the FAST proteins are also structurally distinct from enveloped viral fusion proteins. In particular, at only ~22–44 residues in size, the FAST protein ectodomains are considerably less complex than the ectodomains of enveloped viral fusion proteins. Current models propose that extensive structural remodeling of the large metastable enveloped viral fusion protein ectodomains provides the energy required to drive the fusion reaction (1, 12–15). Because the biophysical features of the FAST proteins are incompatible with a fusion mechanism dependent on dramatic conformational changes in structurally complex ectodomains, alternative models of protein-mediated membrane fusion must be considered. In the case of the 125-residue p14 FAST protein, structural motifs relevant to the membrane fusion activity include the transmembrane domain, a fusion peptide loop and myristate moiety in the 36-residue N-terminal ectodomain, and a membrane-proximal polybasic region in the 68-residue endodomain (4, 9). We currently favor a model of FAST protein-mediated membrane fusion whereby membrane-interactive structural motifs function from either side of the membrane to disrupt the boundary water layer associated with lipid head groups and/or alter lipid packing,

* This work was supported in part by grants from the Canadian Institutes of Health Research (to R. D.) and by grants from the Natural Sciences and Engineering Research Council (to M. H. J.). The costs of publication of this article were defrayed in part by the payment of page charges. This article must therefore be hereby marked "*advertisement*" in accordance with 18 U.S.C. Section 1734 solely to indicate this fact.

[S] The on-line version of this article (available at http://www.jbc.org) contains detailed experimental results and methods for Fig. 1C.

[1] Supported by scholarships from the Natural Sciences and Engineering Research Council, the Cancer Research Training Program of Cancer Care Nova Scotia, and the Nova Scotia Health Research Foundation.

[2] Supported by a scholarship from the Cancer Research Training Program of Cancer Care Nova Scotia.

[3] Recipient of a Regional Partnerships Program Investigator Award from the Canadian Institutes of Health Research. To whom correspondence should be addressed: Dept. of Microbiology and Immunology, Tupper Medical Bldg., Rm. 7S, Dalhousie University, Halifax, Nova Scotia B3H 1X5, Canada. Tel.: 902-494-6770; Fax: 902-494-5125; E-mail: roy.duncan@dal.ca.

thereby lowering the energy barriers that impede membrane fusion (8–11, 16).

The realignment of lipids during the membrane fusion process is believed to proceed through a series of sequential steps involving merger of the outer leaflets of two closely apposed membranes to form a stalk; formation of a hemifusion diaphragm; and then merger of the inner leaflets, leading to pore formation and pore expansion (2, 13). The lipid rearrangements required to achieve these steps are complex and are believed to require the formation of different non-bilayer structures involving negative membrane curvature, acyl chain tilt, and altered lipid packing (13, 17). The liquid-disordered fluid state of biological membranes makes it easy to envision how lipid molecules could be rearranged to form such non-bilayer structures. In recent years, however, the concept of a biological membrane as a fluid mosaic containing randomly dispersed membrane proteins moving through a fluid lipid bilayer has been supplanted by the realization that biological membranes likely contain regions highly biased in both their lipid and protein composition (18). These lipid-based membrane microdomains, so-called "rafts," are currently viewed as small dynamic clusters of protein and lipid enriched in cholesterol and/or sphingomyelin (19). The tight lipid packing promoted by cholesterol and the unsaturated acyl chains present in such membrane microdomains promotes the formation of a liquid-ordered state in model membranes, which may render these lipid microdomains more resistant to detergent solubilization (18, 20). However, the complex interactions between detergents and the lipids and proteins present in membranes make it unclear as to whether the biochemical and biophysical properties of isolated detergent-resistant membranes (DRMs)[4] accurately reflect the properties of membrane microdomains present in native membranes (21–23).

Regardless of the exact relationship between DRMs and actual membrane microdomains, considerable detergent-dependent and -independent analyses support the concept of membrane microdomains with distinct lipid/protein compositions that may serve as organizational centers for numerous proteins (19, 24, 25). In the case of enveloped viral fusion proteins (26), membrane microdomains generally serve as platforms either to concentrate viral glycoproteins in the cell membrane to facilitate viral assembly or to localize viral receptors during the entry process (27–30). If membrane fusion proteins do function from lipid microdomains, then the potential liquid-ordered state of these microdomains may need to be rationalized with the formation of non-bilayer structures that are considered to be essential for the fusion process. It is possible that the fusion proteins migrate out of the microdomains into the more fluid adjacent lipid bilayer during the fusion process, as suggested for influenza virus hemagglutinin, where disruption of membrane microdomains by cholesterol depletion has no adverse effects on the membrane fusion reaction (31). However, theoretical and experimental evidence suggests that some membrane fusion reactions may be mediated within ordered lipid microdomains (32–34). Mechanistic models of membrane fusion may therefore need to adapt to the involvement of liquid-ordered lipid bilayers as a component of the fusion process.

We are particularly interested in understanding how the FAST proteins induce cell-cell fusion. Because the membrane environment from which the FAST proteins mediate the fusion reaction is the cell plasma membrane and in view of the potentially significant impact of the biophysical properties of plasma membrane lipid microdomains on models of the membrane fusion reaction, we determined whether this recently discovered novel family of membrane fusion proteins associates with membrane microdomains. Based on both detergent and non-detergent approaches, our results indicate that the p14 FAST protein associates with distinct membrane microdomains, a subset of which may contain p14 molecules more directly involved in the membrane fusion process.

EXPERIMENTAL PROCEDURES

Cells and Materials—The rabbit anti-p14 polyclonal antiserum and the maintenance of QM5 (quail fibroblast) cells was as described previously (4). N-BP-2 cells are Chinese hamster ovary cell derivatives deficient in cholesterol synthesis because of a deletion in the site-2 protease that activates the sterol regulatory element-binding proteins (35). These cells were obtained from N. Ridgway (Dalhousie University) and were cultured in Dulbecco's modified Eagle's medium supplemented with 5% fetal bovine serum and cholesterol as described previously (36). Anti-placental alkaline phosphatase (PLAP) and anti-human transferrin receptor monoclonal antibodies were purchased from Dako and Zymed Laboratories Inc., respectively. Horseradish peroxidase-conjugated goat anti-mouse and goat anti-rabbit antibodies were obtained from Kirkegaard & Perry Laboratories, Inc. Lubrol WX was purchased from SERVA; all other detergents and cholesterol-depleting reagents (methyl-β-cyclodextrin (MβCD)) were from Sigma. CellTracker dyes were from Molecular Probes.

Expression Plasmids—The authentic p14 and non-myristoylated p14-G2A expression plasmids were as described previously (4). Plasmid vectors expressing PLAP or the human transferrin receptor were generously provided by D. Brown (State University of New York) and C. Parish (Cornell University), respectively. A eukaryotic expression plasmid encoding the vesicular stomatitis virus G protein (VSV-G; Indiana serotype) was provided by P. Lee (Dalhousie University).

Transfection, Cell Staining, and Syncytial Indexing—QM5 quail cell fibroblasts were transfected with p14 expression plasmids using Lipofectamine 2000 (Invitrogen) according to the manufacturer's instructions. At various times post-transfection, cell monolayers were fixed and stained with Wright-Giemsa, and the syncytial index was determined by quantifying the numbers of syncytial nuclei present in random microscopic fields as described previously (4). Results are reported as the means ± S.E. of three separate experiments.

Cholesterol Depletion and Repletion—Membrane cholesterol was depleted from p14-transfected QM5 cells prior to the onset

[4] The abbreviations used are: DRM(s), detergent-resistant membrane(s); PLAP, placental alkaline phosphatase; MβCD, methyl-β-cyclodextrin; VSV-G, vesicular stomatitis virus G protein; cLPDS, complete lipoprotein-deficient serum; HBSS, Hanks' buffered saline solution; PBS, phosphate-buffered saline; AFM, atomic force microscopy; LRMs, Lubrol WX-resistant membranes; TRM(s), Triton X-100-resistant membrane(s); GM1, ganglioside GM1.

of syncytium formation, which commenced at 4–5 h post-transfection, either by acutely treating cells for 30 min with 10–20 mM MβCD in serum-free medium or in medium containing 10% fetal bovine serum or 5% complete lipoprotein-deficient serum (cLPDS) or by incubating cells in medium containing cLPDS and 2 mM MβCD. Following the acute cholesterol depletion treatments, the medium containing MβCD was replaced with complete serum-free medium or with medium supplemented with 5% cLPDS, and cells were incubated for an additional 2–4 h until extensive syncytium formation appeared in the untreated transfected cells. Cells were then fixed, stained, and assessed for syncytium formation as described above. To assess the ability of MβCD to deplete membrane cholesterol, cells were preloaded for 4 h with 5 μCi/ml [^{3}H]cholesterol (ICN), washed with Hanks' buffered saline solution (HBSS), and treated with MβCD under the conditions described above. The cell supernatant was removed; the cell monolayers were lysed in 200 μl of radioimmune precipitation assay buffer (50 mM Tris-HCl (pH 8), 150 mM NaCl, 1 mM EDTA, 1% (v/v) Igepal (Sigma), 0.5% (w/v) sodium deoxycholate, and 0.1% (w/v) SDS); and the percent [^{3}H]cholesterol present in the cell lysate and supernatant was determined by scintillation counting. For cholesterol repletion experiments, cholesterol (6 mg/ml) was dissolved in 20 mM MβCD in serum-free medium by vigorous vortexing and heating at 37 °C for 30 min, filtered to remove insoluble cholesterol, and added to cholesterol-depleted cells for 30 min at 37 °C. In some experiments, the effects of cholesterol depletion on cell-cell fusion mediated by p14 or VSV-G were examined using N-BP-2 cells (cholesterol auxotrophs). Cells were cultured for 12 h in Dulbecco's modified Eagle's medium containing 5% cLPDS with or without cholesterol supplementation as described previously (36). Cells were transfected in the appropriate cholesterol-containing serum-free medium, fixed at 12 h post-transfection (24 h post-cholesterol depletion), Giemsa-stained, and assessed for the extent of cell-cell fusion. Control experiments using fluorescence-activated cell sorter analysis and a green fluorescent protein expression vector indicated no difference in the transfection efficiency of the QM5 cells (63–72%) under the various cholesterol conditions.

Detergent Extraction and Sucrose Density Gradient Centrifugation—10-cm dishes of subconfluent QM5 cells were transfected with p14. After 12–14 h, when syncytium formation was extensive, cells were detached from the substratum with 50 mM EDTA for 15 min; centrifuged at 500 × *g*; and resuspended in 0.5 ml of phosphate-buffered saline (PBS), radioimmune precipitation assay buffer, 0.5% (v/v) Triton X-100, 0.5% (w/v) Lubrol WX (with or without 1 M NaCl), 60 mM octyl glucoside, 0.5% (v/v) Brij 56, or 0.5% (v/v) Brij 58. All detergents were dissolved in 50 mM Tris-HCl (pH 8), 150 mM NaCl, and 1 mM EDTA, and all lysis buffers contained protease inhibitors (200 nM aprotinin, 1 μM leupeptin, and 1 μM pepstatin (Sigma)). When no detergent was used, cells were vesiculated by 20 passes through a 30-gauge needle, and unbroken cells and debris were removed by centrifugation at 700 × *g* for 2 min; when detergent-containing buffer was used, cells were lysed at 4 °C for 30–45 min. Cell lysates (250 μl) were mixed with 250 μl of 2.4 M (82.4%) sucrose and overlaid with 1 ml of 0.9 M (30.8%), 0.5 ml of 0.8 M (27.2%), 1 ml of 0.7 M (24%), and 1 ml of 0.1 M (3.4%) sucrose. Sucrose density gradients were subjected to ultracentrifugation at 332,000 × *g* for 18–20 h and then harvested from the top in 0.5-ml aliquots. The percent sucrose in each fraction was determined using a refractometer. Total protein (0.1 ml of each sucrose fraction) was precipitated using chloroform and methanol and fractionated by SDS-PAGE (15% acrylamide), and proteins were detected by immunoblotting using mouse anti-PLAP or anti-human transferrin receptor monoclonal antibody (1:2000) or rabbit anti-p14 polyclonal antibody (1:10,000) and horseradish peroxidase-conjugated secondary antibody (1:2000–5000). Proteins were visualized by chemiluminescence (ECL, Amersham Biosciences) according to the manufacturer's instructions. The distribution of p14 in the various sucrose fractions was quantified by analysis of scanned Western blots using Scion Image software, and the mean density of individual bands was determined from four to five separate experiments. In some cases, transfected cells were labeled for 1 h with 50 μCi/ml [^{3}H]leucine prior to harvesting, and sucrose fractions were analyzed by immunoprecipitation and SDS-PAGE using rabbit anti-p14 polyclonal antibody as described previously (4).

Fluorescent Heterotypic Cell-Cell Fusion Assays—Individual cell populations were labeled with the dye CellTracker Orange CMTMR (5-(6)-(((4-chloromethyl)benzoyl)amino)-tetramethylrhodamine; 5 μM) or CellTracker Blue CMAC (7-amino-4-chloromethylcoumarin; 2 μM) for 45 min at 37 °C in HBSS following the manufacturer's instructions. Labeled donor cells were transfected with p14 as described above. At 2.5 h post-transfection, donor or target cells were treated with MβCD to deplete cholesterol. The non-depleted cell population was suspended in PBS/EDTA, mixed with 200 μl of fetal bovine serum, pelleted by centrifugation at 700 × *g* for 5 min, resuspended in 100 μl of PBS, mixed with 400 μl of cLPDS, and seeded on monolayers of the labeled cholesterol-depleted cell population grown on coverslips. The two cell populations were incubated for 2 h, washed with HBSS, fixed with methanol, mounted on glass slides using fluorescent mounting medium (Dako), and visualized and photographed using a Zeiss Axiovert 200 fluorescence microscope. The relative number of syncytia per field was determined by counting the number of syncytia in 20–50 random fields using a ×40 objective.

Atomic Force Microscopy (AFM)—Liposomes or proteoliposomes containing purified p14 in the liposome membranes were prepared exactly as described previously (11). Lipid formulations consisted of 1,2-dioleoyl-*sn*-glycero-3-phosphatidylcholine), 1,2-dioleoyl-*sn*-glycero-3-phosphatidylethanolamine, cholesterol, and sphingomyelin at 40:20:20:20 mol %. The fusion activity of p14 present in liposome membranes was confirmed by monitoring liposome-cell membrane fusion as reported previously (11). Supported bilayers were formed by allowing liposomes in 10 mM HEPES (pH 7.5) to attach and then collapse onto freshly cleaved mica surfaces. Following deposition of the lipid bilayers onto the mica surface for at least 2 h at room temperature, AFM images were recorded under aqueous conditions using the contact mode at room temperature with a Molecular Imaging microscope. Images were recorded in both

height and deflection modes. V-shaped cantilevers with oxide-sharpened Si_3N_4 tips (Veeco) were used with spring constants of 0.01 newton-meter as specified by the manufacturer. High resolution images were recorded with optimized feedback parameters at scan frequencies of 4 Hz. Very low forces were applied during the scan, and the threshold for imaging was estimated at ~400 piconewtons. Images were obtained from at least three different samples prepared on different days, and several macroscopically separate areas were scanned on each sample. Several images were analyzed from each experiment, and ~100 AFM cross-section profiles were used to estimate the height of the observed membrane microdomains and p14 protein spikes (height of the microdomains = 0.8 ± 0.2 nm (n = 30) and height of the spikes = 1.5 ± 0.5 nm (n = 70)).

Surface Fluorescence Microscopy and Co-localization—QM5 cells grown on coverslips were transfected or cotransfected and stained for surface immunofluorescence. For cotransfection experiments, the non-fusogenic p14 construct (p14-G2A) was used to prevent syncytium formation and to allow expression of PLAP. At 24 h post-transfection, cells were preblocked with whole goat IgG (1:1000) in HBSS for 30 min at 4 °C, treated with primary antibody (rabbit anti-p14 polyclonal antibody (1:200) and/or mouse anti-PLAP monoclonal antibody (1:50) in the blocking buffer) for 60 min at 4 °C, washed with HBSS, and then treated with secondary antibody (Alexa Fluor 488- or Alexa Fluor 555-conjugated goat anti-mouse and/or goat anti-rabbit IgG (1:200; Molecular Probes) in the blocking buffer). After secondary antibody addition and washing, cells were fixed with 3.7% formaldehyde in PBS and mounted on glass slides using fluorescent mounting medium. GM1 was stained using Alexa Fluor 555-conjugated cholera toxin B (0.1 μg/ml) during the primary antibody incubation. After washing as described above, anti-cholera toxin B antibody (1:200) was added during the secondary antibody incubation to cause individual GM1 molecules on the cell surface to coalesce (37). Stained cells were visualized and photographed using a Zeiss LSM 510 META scanning argon laser confocal microscope and a ×100 objective.

Thin Layer Chromatography—Untransfected or p14-transfected QM5 cells were labeled with 10 μCi of [^{14}C]acetate/dish (10^7 cells) for 16–18 h. After labeling, cells were left untreated or treated with MβCD for cholesterol depletion/repletion as described above and extracted with Lubrol WX or Triton X-100 prior to isolation of DRMs by sucrose density gradient ultracentrifugation as described above. Total lipid from each fraction or fraction pool was isolated using 2:1 (v/v) chloroform/methanol (38), and aliquots of the lipid extract containing equal amounts of radioactivity (20,000 dpm) were applied to Silica Gel G plates (Macherey-Nagel). Cholesterol and phospholipids were fractionated by thin layer chromatography using a 24:30:6:30 (v/v/v/v) chloroform/ethanol/water/triethylamine mobile phase as described previously (39). Phospholipid/cholesterol standards were run in parallel and detected by treatment with sulfuric acid and charring at 180 °C. The percentage of radioactivity recovered in each lipid spot was quantified using a Model GS-525 molecular imager system and Molecular Analyst 1.5 software (Bio-Rad).

RESULTS

p14-induced Membrane Fusion Is Sensitive to Donor Membrane Cholesterol Levels—In view of the importance of the lipid environment to membrane fusion and the absence of any information on the effect of this environment on the function of the recently discovered FAST proteins, we examined the influence of cholesterol on syncytium formation induced by the p14 FAST protein. QM5 fibroblasts were transfected with a p14 expression plasmid, and membrane cholesterol was depleted with MβCD prior to the onset of cell-cell fusion. Quantitative analysis indicated that MβCD extracted 60–90% of the membrane cholesterol under various extraction conditions (Fig. 1*D*) and that p14-induced syncytium formation was inhibited by 80–90% under all conditions (Fig. 1, *A* and *B*). Furthermore, restoration of membrane cholesterol by treatment of cells with cholesterol-loaded MβCD substantially restored the rate of syncytium formation (Fig. 1*C*). Accounting for the 60-min lag between the time course of syncytium formation in treated *versus* untreated cells (*i.e.* the time course of syncytium formation in treated cells was delayed by the cholesterol depletion and repletion steps), cholesterol repletion essentially restored p14-induced syncytium formation to the levels observed in untreated cells (data not shown).

To control for possible indirect effects of cholesterol depletion on p14-mediated cell-cell fusion, we examined the effects of acute cholesterol depletion by MβCD on the cell-cell fusion activity of the VSV-G fusion protein. Although VSV-G does not appear to associate with lipid microdomains based on detergent fractionation analysis (29), the effects of cholesterol depletion by MβCD on VSV-G cell-cell fusion activity have never been reported. To serve as a suitable control for p14 inhibition by cholesterol depletion, rather than using low pH treatment to trigger VSV-G fusion activity, we exploited the fact that transient overexpression of VSV-G in cells that partially acidify the medium results in gradual cell-cell fusion. This phenotype parallels the progressive fusion activity of the FAST proteins, which are untriggered fusogens. As shown in Fig. 1*C*, cell-cell fusion mediated by VSV-G was completely unaffected by acute cholesterol depletion conditions that inhibited p14 fusion activity by >80%.

We also examined p14 fusion activity in N-BP-2 cells, a cholesterol auxotrophic cell line (35). Under conditions in which N-BP-2 cells are deficient in membrane cholesterol (24 h of cholesterol depletion), p14-induced cell-cell fusion was inhibited by ~50% (Fig. 1*C*). However, the same experimental conditions resulted in ~70% inhibition of VSV-G cell-cell fusion both when VSV-G fusion occurred under the neutral pH conditions described above (data not shown) and when fusion was triggered by low pH treatment (Fig. 1*C*). The different effects of the two cholesterol depletion protocols (*i.e.* MβCD or auxotrophic cells) on VSV-G fusion activity most likely reflect differences in the cellular response to acute *versus* extended cholesterol depletion.

Because cholesterol depletion can exert its effect on membrane fusion proteins from either the donor or target membrane (30, 34, 40), we used a fluorescent heterotypic cell-cell fusion assay and acute cholesterol depletion with MβCD to

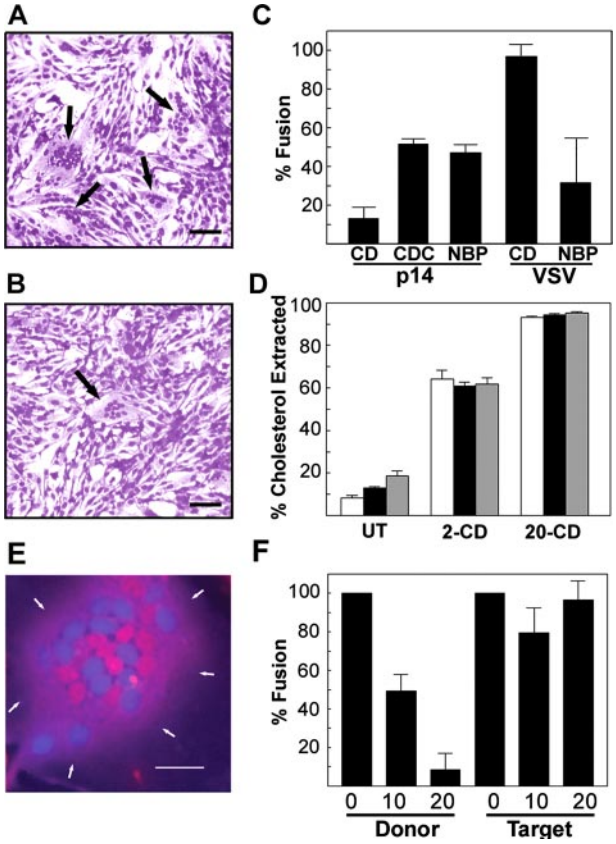

FIGURE 1. **p14-induced syncytium formation is influenced by membrane cholesterol in the donor membrane.** *A* and *B*, p14-transfected QM5 cells were left untreated or were treated, respectively, with 2 mM MβCD in medium containing 5% cLPDS just prior to and during syncytium formation. Cells were Giemsa-stained and observed under a light microscope for the appearance of multinucleated syncytia. *Arrows* in *A* indicate numerous syncytial foci. The *arrow* in *B* indicates a single small syncytium. *Scale bars* = 100 μm. *C*, QM5 cells transfected with the p14 or VSV-G expression plasmid were treated for 30 min with 10 mM MβCD (*CD*) just prior to the onset of syncytium formation. A sample of p14-transfected, MβCD-treated QM5 cells was subsequently supplemented with exogenous cholesterol for 30 min at 37 °C using MβCD-cholesterol complexes (*CDC*). All cells were maintained in serum-free medium at 37 °C for an additional 2–4 h. Similar studies were performed in p14- or VSV-G-transfected N-BP-2 cells (*NBP*), except that cholesterol depletion was induced by culturing these cholesterol auxotrophs under cholesterol-limiting conditions for 24 h as described under "Experimental Procedures." At the completion of each experiment, cells were Giemsa-stained, and the average number of nuclei present in syncytia was determined by microscopic examination of five random fields and used to determine the percent fusion relative to untreated cells. Results are expressed as the means ± S.E. of three separate experiments, except for the VSV-G results in N-BP-2 cells, which are the means ± S.D. of a single experiment. Results from the replicate experiments are provided in the supplemental material. *D*, p14-transfected QM5 cells were prelabeled with [^{3}H]cholesterol and then left untreated (*UT*) or treated with 2 or 20 mM MβCD (*2-CD* and *20-CD*, respectively) in serum-free medium (*white bars*), 5% cLPDS (*black bars*), or 10% fetal bovine serum (*gray bars*). The percent [^{3}H]cholesterol extracted from the cells by MβCD was quantified by scintillation counting. *E*, untransfected QM5 cells prelabeled with CellTracker Blue CMAC (*blue*) were co-cultured with p14-transfected cells prelabeled with CellTracker Orange CMTMR (*red*). Fluorescence microscopy revealed the presence of syncytial foci containing both red and blue cell nuclei, indicating that p14-transfected donor cells fuse to untransfected target cells. *Scale bar* = 30 μm. *Arrows* indicate the edges of a single syncytium. *F*, the same experiment as described for *E* was conducted, except that p14-transfected donor cells or untransfected target cells were treated with 0, 10, or 20 mM MβCD prior to co-culturing the two cell populations. The number of syncytial nuclei per field was determined by counting random microscopic fields and used to calculate the percent fusion relative to the untreated sample. Results are the means ± S.E. of three experiments.

examine the influence of donor *versus* target membrane cholesterol levels on p14-mediated cell-cell fusion. p14-transfected cells (donor membranes) and untransfected cells (target membranes) were fluorescently labeled with different CellTracker dyes, depleted of cholesterol using 10 or 20 mM MβCD, and then co-cultured and monitored for cell-cell fusion. Quantifying the formation of heterotypic syncytia (*i.e.* syncytia containing both donor (Fig. 1*E*, *red*) and target (*blue*) nuclei) revealed that depletion of donor membrane cholesterol resulted in a dose-dependent decrease in p14-induced syncytium formation (>90% inhibition), whereas depletion of target membrane cholesterol had little, if any, significant effect on syncytium formation (Fig. 1*F*). The cell-cell fusion activity of p14 therefore appears to be sensitive to the cholesterol content of the membrane in which p14 resides.

p14 Associates with Detergent-resistant Membranes in a Myristoylation-independent Manner—The donor membrane cholesterol dependence of p14-induced syncytium formation suggested that p14 might localize to cholesterol-rich membrane microdomains. In accord with this possibility, a significant proportion of p14 remained detergent-insoluble when cells were extracted with the non-ionic detergents Triton X-100, Lubrol WX, Brij 56, and Brij 58 (Fig. 2*A*). Qualitative assessments indicated that p14 exhibited differential resistance to solubilization by the different detergents, with the greatest proportion of insoluble p14 observed following Lubrol WX extraction. The inclusion of high salt in the lysis buffer did not disrupt the Lubrol WX-insoluble nature of p14, whereas treatment of cells with octyl glucoside, which tends to preserve cytoskeleton-associated membrane proteins but solubilizes membrane microdomains (41, 42), rendered p14 completely soluble (Fig. 2*A*), suggesting that p14 association with DRMs is not due to residual cytoskeletal interactions.

Sucrose density gradient centrifugation confirmed the association of p14 with DRMs as evidenced by the migration of a proportion of the Triton X-100- and Lubrol WX-insoluble p14 to the low density 10–20% sucrose fractions (Fig. 2*B*). The presence of p14 in DRMs was not due to inadequate detergent/lipid or detergent/protein ratios required to efficiently solubilize membranes, as indicated by the complete solubilization by Lubrol WX of the transferrin receptor, an archetypal membrane protein that does not associate with DRMs (Fig. 2*B*). In contrast to PLAP, a glycophosphatidylinositol-linked microdomain-associated protein which localized exclusively to the low density DRM sucrose fractions, p14 exhibited a broad and somewhat variable (*e.g.* compare Figs. 2*B* and 3) density distribution following extraction with either Triton X-100 or Lubrol WX, a profile similar to that of numerous other microdomain-associated transmembrane proteins (43–46). Quantitative analysis of p14 distribution in the sucrose density fractions based on pixel analysis of the fluorograms from four to five individual experiments indicated that, on average, approximately half of the total p14 present in detergent cell lysates was associated with DRMs, with the remainder distributed throughout the intermediate and high density sucrose fractions (Fig. 2*C*). The fact that Lubrol WX solubilized more p14 compared with Triton X-100 (*i.e.* 38 and 20% of p14 were found in the soluble high density sucrose fractions following extraction

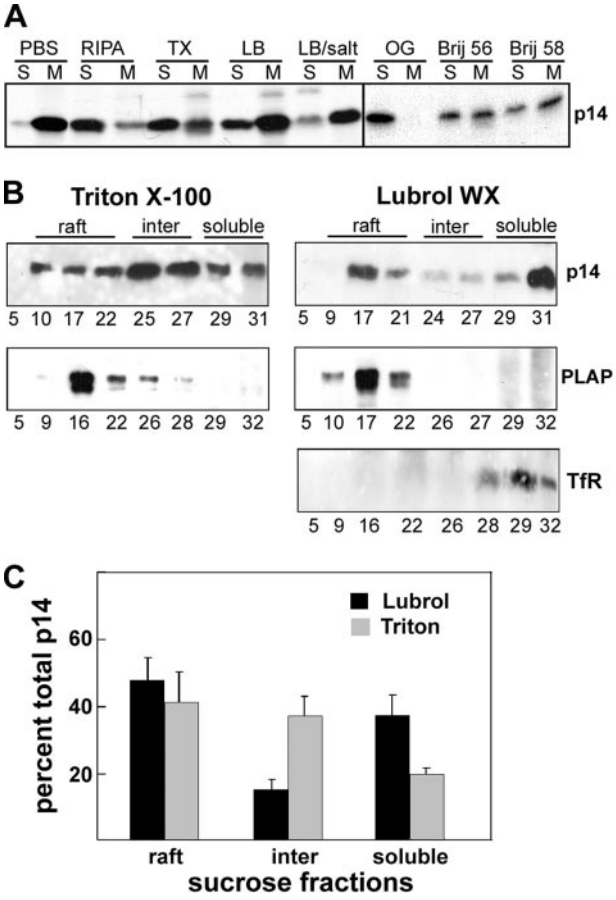

FIGURE 2. **p14 associates with both Lubrol WX- and Triton X-100-resistant membranes.** *A*, radiolabeled p14-transfected QM5 cells were treated with PBS, radioimmune precipitation assay (*RIPA*) buffer, 0.5% Triton X-100 (*TX*), 0.5% Lubrol WX (*LB*), 0.5% Lubrol WX in 1 M NaCl (*LB/salt*), 60 mM octyl glucoside (*OG*), 0.5% Brij 56, or 0.5% Brij 58 on ice for 45 min. Cell extracts were fractionated into soluble (*S*) and insoluble membrane (*M*) fractions by ultracentrifugation, and the presence of p14 in each fraction was detected by immunoprecipitation, SDS-PAGE, and fluorography. *B*, p14-, PLAP-, or human transferrin receptor (*TfR*)-transfected QM5 cells were lysed with either 0.5% Triton X-100 (*left panels*) or 0.5% Lubrol WX (*right panels*) and subjected to sucrose density gradient ultracentrifugation. Sucrose fractions were analyzed for the presence of protein by SDS-PAGE and immunoblotting with anti-p14, anti-PLAP, or anti-human transferrin receptor antibody. The percent sucrose present in each fraction of the gradient is indicated below the corresponding panel. *C*, the percentage of total p14 protein present in the pooled raft, intermediate (*inter*), and soluble fractions from sucrose gradients similar to those in *B* was quantified using Scion Image software, and results are presented as the means ± S.E. of four to five separate experiments.

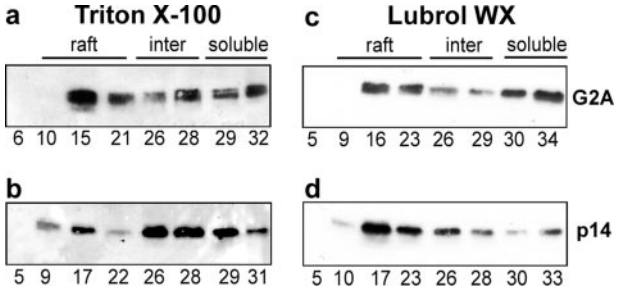

FIGURE 3. **p14 association with DRMs is myristoylation-independent.** QM5 cells transfected with authentic p14 (*b* and *d*) or non-myristoylated p14-G2A (*a* and *c*) were lysed with either Triton X-100 (*a* and *b*) or Lubrol WX (*c* and *d*) and subjected to sucrose density gradient ultracentrifugation. Sucrose fractions were analyzed for the presence of p14 by SDS-PAGE and immunoblotting with anti-p14 polyclonal antibody. The percent sucrose in each fraction of the gradient is indicated below the corresponding panel. *inter*, intermediate density sucrose fraction.

with Lubrol WX and Triton X-100, respectively) argues against the concern that Lubrol WX is a less efficient detergent than Triton X-100 and therefore not useful for identifying microdomain-associated proteins (47). Both the detergent resistance and cholesterol sensitivity of p14 were suggestive of p14 association with membrane microdomains.

Because myristate can serve as a targeting signal for membrane microdomains (41), the demonstration that p14 associates with DRMs provided a possible explanation for the essential role of N-terminal myristoylation in the fusion activity of p14 (4). However, analysis of a previously characterized non-myristoylated construct of p14, p14-G2A (9), indicated that this was not the case; aside from slight variations between experiments in the relative distribution of p14 in the low and intermediate density sucrose fractions, the p14-G2A construct displayed the same general distribution in sucrose gradients as authentic p14 (Fig. 3). The p14 protein therefore associates with DRMs (and by inference, membrane microdomains in cells) in a myristoylation-independent manner.

Preferential Association of p14 with Lipid Microdomains—Although detergent insolubility serves as the most common operational definition of a microdomain-associated protein, the uncertain nature of the relationship between DRMs and functional membrane microdomains complicates this simple interpretation (19, 21–23). Detergent-independent evidence for p14 association with lipid microdomains was therefore obtained by AFM using supported lipid bilayers containing p14. Following deposition of lipid vesicles onto mica surfaces, the liposomes flatten and merge to form double bilayer discs that subsequently rupture to form a continuous supported phospholipid bilayer (48). Such supported bilayers provide a platform for the analysis of membrane proteins under near-physiological conditions and have been used recently in conjunction with AFM to study lipid microdomains and microdomain-associated proteins (49–51). AFM is based on scanning the surface of mica-supported lipid bilayers using a sharpened Si_3N_4 probe attached to a flexible cantilever. Vertical deflections of the probe are detected and used to map the surface contour of the membrane at very high resolution (<1 nm) (52). We demonstrated recently that purified p14 reconstituted into 400 nm liposomes composed of a model mixture of membrane lipids (1,2-dioleoyl-*sn*-glycero-3-phosphatidylcholine/1,2-dioleoyl-*sn*-glycero-3-phosphatidylethanolamine/cholesterol/sphingomyelin at 40:20:20:20 mol %) mediates efficient liposome-cell fusion, indicating that p14 in these liposomes resides in a fusion-competent membrane environment (11). We therefore used these fusogenic liposomes to generate supported lipid bilayers, and the surface topography of the bilayers was examined by high resolution AFM under aqueous conditions.

Membrane microdomains spontaneously formed in protein-free lipid bilayers and were readily observed by AFM as discrete patches of membrane extending ~0.8 ± 0.2 nm above the lipid bilayer (Fig. 4, *A–C*). The difference in height of the membrane microdomains and surrounding lipid bilayer approximated the difference in length between 1,2-dioleoyl-*sn*-glycero-3-phos-

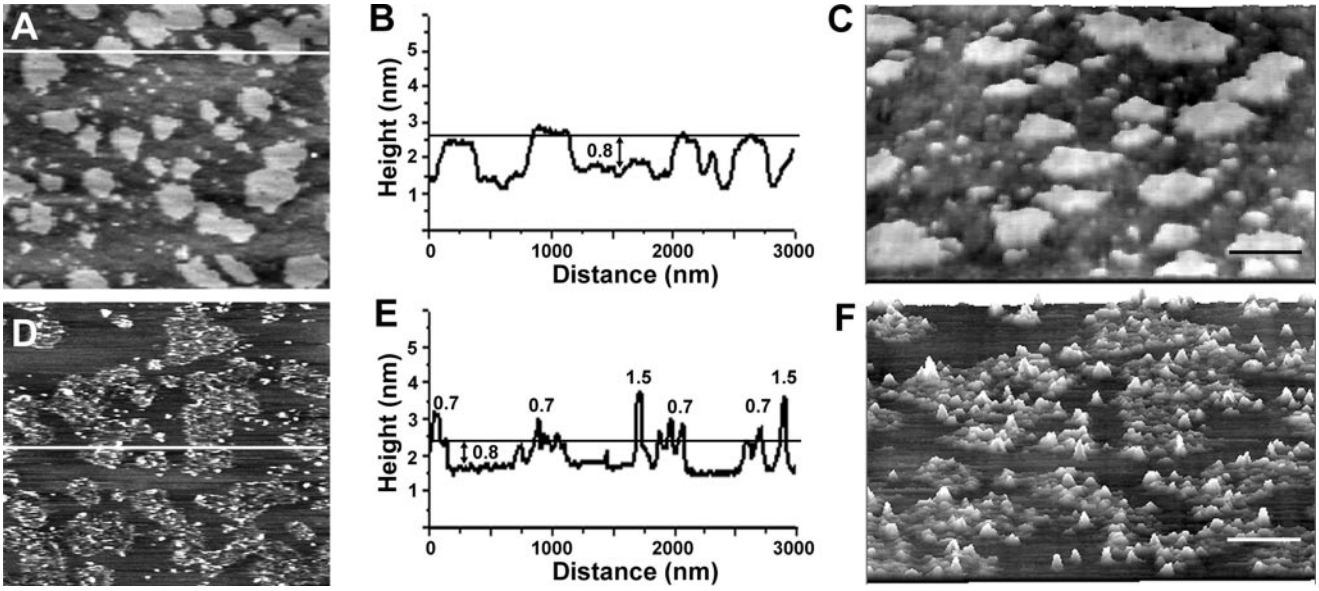

FIGURE 4. **p14 associates with membrane microdomains under aqueous conditions.** AFM images were obtained from supported lipid bilayers prepared from liposomes either lacking (*A–C*) or containing (*D–F*) purified p14. The images in *A* and *D* were taken from above, and height projections were color-matched (lowest to highest corresponds to *black* to *white*). The *black* background represents the lipid bilayer; the *gray* regions correspond to raised lipid microdomains; and the *white* spots in *D* correspond to protrusions projecting above the height of the lipid microdomains in the p14-containing bilayers. The *horizontal white lines* in *A* and *D* indicate the AFM tracing used to obtain the corresponding virtual cross-section profiles of each AFM image presented in *B* and *E*. The *horizontal lines* in *B* and *E* denote the height of the lipid microdomains above the lipid bilayers. *Numbers* indicate height differences (in nanometers) of the indicated topographical features. The surface contours of the bilayers are presented in three-dimensions in *C* and *F*, showing the raised lipid microdomains containing the protruding p14 protein spikes. *Scale bars* = 300-nm horizontal distance (*C* and *F*).

phatidylcholine and sphingomyelin molecules, suggesting that these microdomains are enriched in sphingomyelin and likely exist in a liquid-ordered phase. These results were in good agreement with previous AFM reports on the spontaneous formation and thickness of cholesterol- and/or sphingomyelin-rich lipid microdomains in supported lipid bilayers (49, 50, 53). The lipid microdomains were heterogeneous in size, ranging from ~50 to 500 nm in diameter, a size distribution that probably reflects lateral mobility and merger of smaller microdomains during the transition from liposomes to a supported bilayer (50). Microdomains with similar two-dimensional proportions were observed in supported lipid bilayers that contained p14, although their surface topography was markedly altered by the presence of numerous protrusions extending above the height of the membrane microdomains (Fig. 4, *D–F*). Such protrusions were never observed in the membranes of protein-free liposomes, suggesting that they represent the p14 protein. When viewed from above, the protrusions were visible in the shaded height projection as white spots (Fig. 4*D*). In cross-sections, the protrusions projected ~1.5 ± 0.5 nm above the surface of the microdomains, which themselves extended ~0.8 nm above the lipid bilayer (Fig. 4*E*). When viewed in three dimensions (Fig. 4*F*), the protrusions appeared as distinct spikes, similar in appearance although smaller in height (*i.e.* 1.5 *versus* 10 nm) than the microdomain-associated spikes of the much larger PLAP protein previously observed by AFM (49). Most notable was the fact that the majority of the p14 protein spikes were found associated with the thickened membrane microdomain platforms. This is evident from the preferential association of the white spots with the obvious microdomain platforms in the lower magnification two-dimensional shaded height projection (Fig. 4*D*) and by the clustering of the protein spikes in the higher magnification three-dimensional projection (Fig. 4*F*).

The high resolution of AFM revealed further complexity in the surface topography of the p14-containing lipid microdomains. In addition to the increased variations in height conferred by the prominent 1.5-nm tall protein spikes, a second series of what appeared to be shorter protrusions was observed in the microdomains containing p14. The height of these smaller projections averaged ~0.7 nm above the lipid microdomains (Fig. 4*E*). In the three-dimensional image, these smaller protrusions imparted a more irregular surface to the p14-containing lipid microdomains (Fig. 4*F*). We suggest that these two populations of protrusions most likely represent two topologies of p14 in liposome membranes (both the correct N-exoplasmic/C-cytoplasmic and the inverse C-exoplasmic/N-cytoplasmic topology), as indicated previously by flow cytometry of p14-containing liposomes using anti-p14 N and C termini-specific antisera (11). Support for this conjecture derives from the ~2-fold difference in the size of the p14 N-terminal ectodomain and C-terminal endodomain (*i.e.* 36 *versus* 68 residues), which closely mirrors the 2-fold difference in the average heights of the projections (*i.e.* 0.7 *versus* 1.5 nm). The AFM results provide compelling detergent-independent evidence that p14 preferentially associates with lipid microdomains under aqueous conditions.

Distinct Populations of p14-containing Detergent-resistant Membranes—Further analysis of the detergent solubility of p14 extracted from transfected cells unveiled two additional notable features of p14 association with DRMs. The first related to the approximately equivalent percentages of p14 associated with either Lubrol WX-resistant membranes (LRMs) or Triton X-100-resistant membranes (TRMs) (Fig. 2, *B* and *C*). This

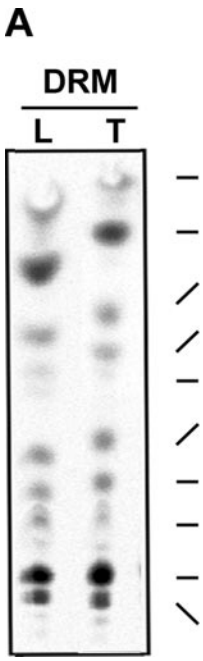

Lipid	% DRM Lipid	
	Lubrol	Triton
NLs	**6.0** 6.1 5.9	**4.2** 4.9 3.5
Chol	**27.2** 26.0 28.3	**20.4** 19.8 20.9
Glu-cer	**3.3** 5.5 1.2	**4.7** 4.5 4.8
Gal-cer	**1.8** 2.0 1.6	**2.8** 3.2 2.4
?	**0.3** 0.6 0.0	**0.4** 0.6 0.2
PE	**7.7** 5.6 9.9	**7.7** 5.5 9.9
PI	**3.9** 3.8 4.0	**4.4** 4.3 4.4
PS/Lac-cer	**3.9** 3.5 4.3	**2.0** 1.7 2.2
PC	**35.4** 35.9 34.8	**44.9** 46.0 43.8
Sph	**10.5** 11.0 10.1	**8.7** 9.5 7.8

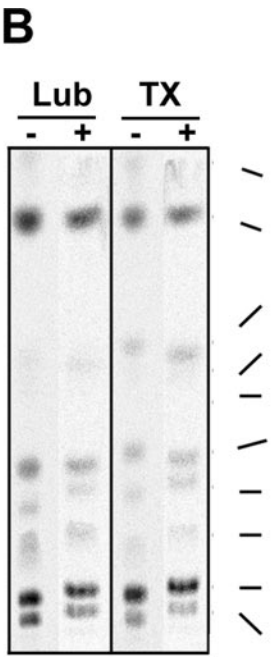

Lipid	Lubrol		Triton	
	-p14	+p14	-p14	+p14
NLs	5.1	7.5	3.7	5.1
Chol	23.7	22.9	19.5	20.4
Glu-cer	1.5	5.1	5.6	8.1
Gal-cer	2.2	2.3	1.3	2.2
?	0.2	0.5	0.2	0.4
PE	10.0	9.4	8.1	8.2
PI	4.4	4.8	4.1	6.0
PS/Lac-cer	3.9	4.0	2.7	2.6
PC	38.1	33.6	44.6	38.7
Sph	10.9	9.8	10.3	8.4

FIGURE 5. **Lipid profiles of LRMs and TRMs.** *A*, untransfected QM5 cells were radiolabeled with [^{14}C]acetate. After sucrose density gradient ultracentrifugation of Lubrol WX (*L*)- or Triton X-100 (*T*)-extracted membranes, the low density DRM fractions (fractions 2–4) were pooled, and total lipids were fractionated by thin layer chromatography and detected by fluorography. Each lipid was identified by comparison with known standards that were run in parallel. The amount of radioactivity corresponding to each lipid was quantified and is displayed in the corresponding *table*. Values are reported for two independent experiments, along with the average (*boldface*). *NLs*, neutral lipids; *chol*, cholesterol; Glu-cer: glucosylceramide; *Gal-cer*, galactosylceramide; *?*, unidentified phospholipid; *PE*, phosphatidylethanolamine; *PI*, phosphatidylinositol; PS/Lac-cer, phosphatidylserine/lactosylceramide; *PC*, phosphatidylcholine; *Sph*, sphingomyelin. *B*, untransfected (−) or p14-transfected (+) QM5 cells were radiolabeled with [^{14}C]acetate, lysed with either Lubrol WX (*Lub*) or Triton X-100 (*TX*), and fractionated by sucrose density gradient ultracentrifugation. The lipid contents of the DRM fractions were analyzed by thin layer chromatography as described for *A*. The amount of radioactivity corresponding to each lipid was quantified and is displayed in the corresponding *table*. Values are reported for a single experiment.

observation appeared to be at odds with previous studies suggesting that LRMs and TRMs contain distinct subpopulations of membrane microdomains that differ both in their lipid composition and in the proteins that preferentially associate with them (43–45, 54). However, other proteins that associate with both types of DRMs have been identified, suggesting that certain proteins may not be as restricted in their choice of compatible lipid environments (43, 46, 55). To determine whether this latter case applies to p14, thin layer chromatography was used to ascertain whether the DRMs isolated with the different detergents were compositionally distinct. As shown in Fig. 5*A*, LRMs isolated from quail cells contained slightly more cholesterol and sphingomyelin (27 *versus* 20% and 11 *versus* 9%, respectively) and less phosphatidylcholine (35 *versus* 45%, respectively) compared with TRMs, percentages that were reasonably consistent in two independent experiments. Furthermore, the relative lipid compositions of the DRMs obtained from untransfected cells extracted by the two detergents were similar to those observed in identical fractions obtained from p14-transfected cells extracted in the same manner, particularly in regard to their cholesterol and sphingomyelin content (Fig. 5*B*). Differences were noted in some of the more minor lipid components (*e.g.* glucosylceramide). These results suggest that the effect, if any, of p14 recruitment of a specific subset of membrane lipids into DRMs is moderate and indicate that p14 can associate with biochemically distinct DRM environments. This latter point does not imply that the different detergents extract intact membrane microdomains, merely that p14 can associate with distinct lipid environments.

The second notable feature of p14 segregation between detergent-soluble and -insoluble fractions became apparent following analysis of the effects of cholesterol depletion/repletion on p14 resistance to detergent extraction. In four to five separate experiments, cholesterol depletion led to an average 50% decrease in the proportion of p14 found in the LRMs and a concomitant increase in the percentage of soluble p14 in the high density sucrose fractions. Subsequent restoration of membrane cholesterol redistributed p14 back into the Lubrol WX-resistant low density sucrose fractions (Fig. 6, *B* and *C*). Such was not the case with TRMs; cholesterol depletion/repletion had little, if any, effect on redistributing p14 between the soluble and TRM fractions (Fig. 6, *A* and *C*). The same situation applied to PLAP (*i.e.* cholesterol-dependent association with LRMs, but not TRMs) and has been previously noted for the association of PLAP and other membrane proteins with TRMs (56–58). We noted that the differential effect of cholesterol depletion/repletion on p14 association with LRMs (but not TRMs) correlated both with the increased cholesterol content of LRMs (Fig. 5) and with the inhibitory effects of cholesterol depletion on p14-induced cell-cell fusion (Fig. 1*C*). The cholesterol depletion/repletion studies indicated that p14 associates with biochemically distinct subsets of membrane microdomains, one or more of which are partially resistant to Lubrol WX extraction and which may contain a subpopulation of p14 actively involved in the cell-cell fusion process.

Further detergent-independent evidence that p14 associates with heterogeneous membrane microdomains was obtained by fluorescence microscopy. Patching of surface-

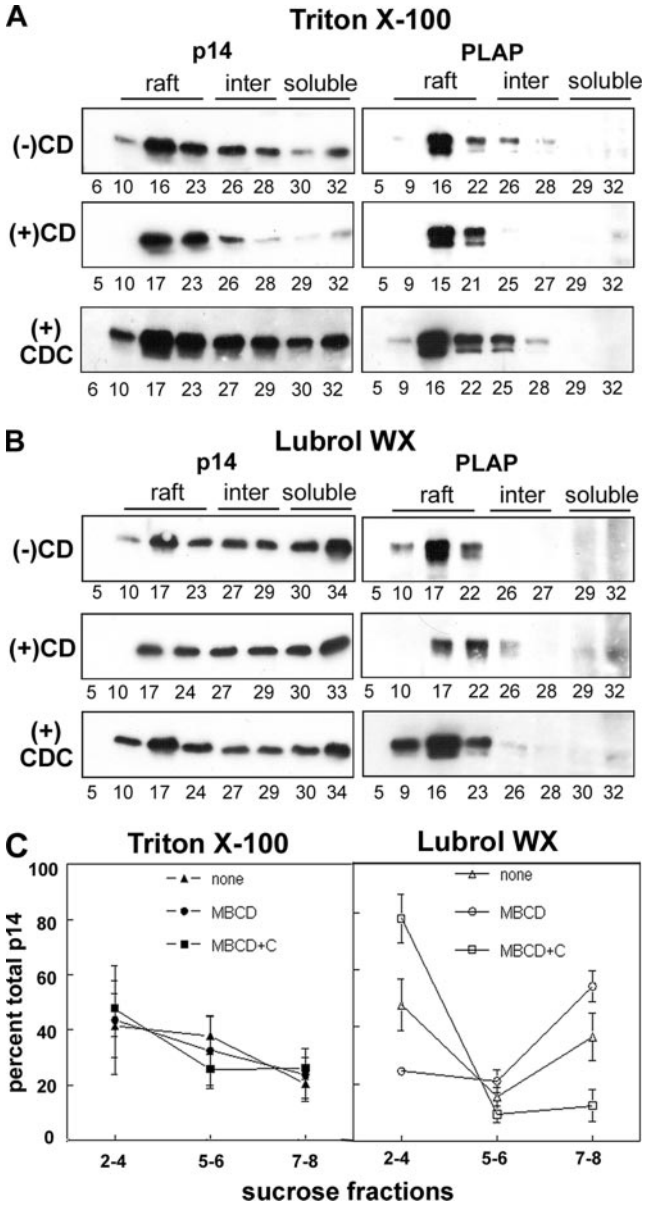

FIGURE 6. **p14-containing LRMs are sensitive to cholesterol depletion.** *A* and *B*, p14- or PLAP-transfected QM5 cells were lysed with either Triton X-100 or Lubrol WX, respectively. After sucrose density gradient ultracentrifugation, fractions of each gradient were analyzed for the presence of protein by SDS-PAGE and immunoblotting with anti-p14 polyclonal or anti-PLAP monoclonal antibody. In each experiment, prior to detergent extraction, cells were either left untreated (*(−)CD*) or were treated with 20 mM MβCD (*(+)CD*) or with MβCD followed immediately by cholesterol repletion using MβCD-cholesterol complexes (*(+)CDC*). The percent sucrose in each fraction of the gradient is indicated below the corresponding panel. *inter*, intermediate density sucrose fraction. *C*, the percentage of total p14 protein in pooled fractions from sucrose gradients similar to those in *A* and *B* was quantified using Scion Image software. *Fractions 2–4*, low density DRM fractions; *fractions 5–6*, intermediate density fractions; *fractions 7–8*, soluble high density fractions. Results are displayed graphically and represent the means ± S.E. of four to five separate experiments. *MBCD*, MβCD; *MBCD+C*, MβCD-cholesterol complexes.

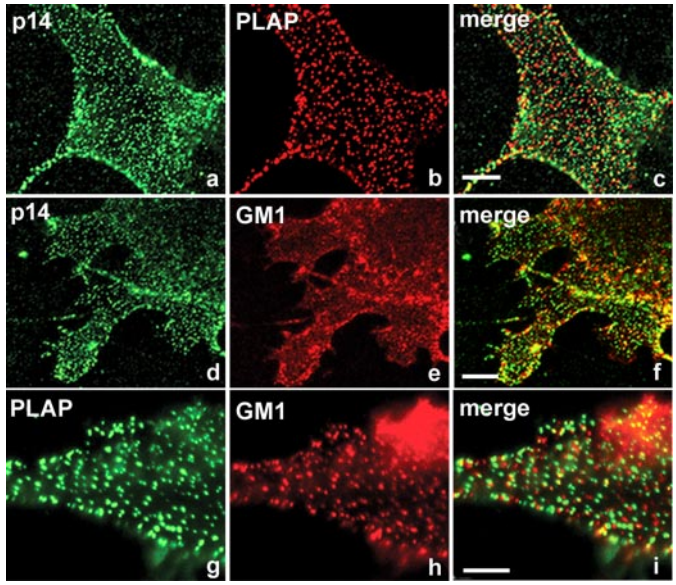

FIGURE 7. **p14 does not co-localize with classical raft markers.** In *a–c*, cells were cotransfected with PLAP and the non-fusogenic p14-G2A construct so as to prevent syncytium formation and to allow sufficient time for PLAP expression. Unfixed cells were surface-stained using anti-p14 polyclonal and anti-PLAP monoclonal antibodies and fluorescently tagged secondary antibodies prior to fixation. *c* is the merged image of *a* and *b*. In *d–f*, cells were transfected with authentic p14 and stained using anti-p14 polyclonal antibody and fluorescently tagged secondary antibodies, and the endogenous ganglioside GM1 was patched and detected using fluorescently conjugated cholera toxin B and anti-cholera toxin antibody. *f* is the merged image of *d* and *e*. In *g–i*, cells were transfected with PLAP, and PLAP and GM1 were patched and detected as described above. *i* is the merged image of *g* and *h*. *Scale bars* = 10 μm.

expressed p14 with anti-p14 polyclonal antiserum prior to fixation did not result in obvious co-localization with the glycophosphatidylinositol-linked protein PLAP, similarly clustered using anti-PLAP antibody, or with the sphingolipid GM1, clustered using subunit B of cholera toxin and anti-cholera toxin antibody (Fig. 7). Aside from a very low level of co-localization, one might expect, on a purely random basis, the majority of p14 to appear in clusters that do not overlap with patches containing either PLAP or GM1, suggesting that p14 associates with subsets of membrane microdomains that may be distinct from those containing certain classical raft markers. Interestingly, although PLAP and GM1 have been reported to co-patch in T cells (37), they did not co-localize following patching in QM5 cells (Fig. 7, *g–i*). A similar lack of co-patching of microdomain-associated proteins has been noted in other systems (59, 60), results consistent with the emerging view that membrane microdomains are most likely heterogeneous, small, and dynamic structures. Consequently, proteins that transiently associate with the same microdomain would not necessarily co-patch following antibody-mediated clustering. Alternative approaches such as fluorescence resonance energy transfer might address whether p14 transiently associates with other microdomain-associated proteins.

DISCUSSION

Biochemical, microscopic, and morphological analyses support the concept that p14 preferentially associates with membrane microdomains with features (*i.e.* sensitivity to cholesterol depletion and detergent insolubility) that are consistent with cholesterol- and/or sphingolipid-enriched microdomains. The AFM results also indicated that p14 can associate, at least in model membranes, with lipid microdomains that likely exist in a liquid-ordered phase. The association of p14 with membrane

microdomains has important implications for models of p14-induced membrane fusion.

As an aside, we have also shown, for the first time, that the cell-cell fusion activity of VSV-G is unaffected by acute cholesterol depletion, an observation consistent with the designation of VSV-G as a "non-raft" membrane protein. Cholesterol depletion using the auxotrophic N-BP-2 cells resulted, however, in substantial inhibition of VSV-G fusion activity. This contrasts with previous results indicating that VSV-G can induce cell-cell fusion in other cholesterol-deprived cell types (61). The discrepancies in the cholesterol dependence of VSV-G fusion activity presumably reflect different pleiotropic effects arising from the various approaches used to deplete membrane cholesterol (*i.e.* acute chemical depletion *versus* extended cholesterol deprivation in different cell types). These results suggest that, at least for VSV-G, acute chemical depletion may be a preferred approach for depleting membrane cholesterol.

Our data also suggest that p14 is an example of a microdomain-associated protein that can be extracted into biochemically distinct DRM environments, one of which is operationally defined by cholesterol-dependent resistance to extraction with Lubrol WX; displacement of p14 from these Lubrol WX-resistant membranes coincided with the inhibition of p14-induced cell fusion. On the basis of these observations, we propose that p14 localizes to membrane microdomains that exhibit heterogeneity in their biophysical properties and that a subset of these microdomains may be more relevant to the process of p14-induced syncytium formation.

In addition to the standard detergent extraction and cholesterol depletion approaches most commonly employed to define microdomain-associated proteins, we exploited our recently developed fusogenic p14-containing liposome system and the high resolution of AFM to reveal the preferential association of functional p14 with lipid microdomains under aqueous conditions (Fig. 4). Supported planar lipid bilayers have been employed under aqueous conditions in conjunction with AFM to provide important insights into the spontaneous formation of lipid microdomains and the association of purified proteins with these microdomains (49–51, 53, 62, 63). Such was the case in this study, in which we observed the spontaneous formation of microdomains with a projection above the lipid bilayer that closely corresponded with previous estimates on the thickness of cholesterol- and/or sphingomyelin-enriched lipid microdomains. The clear presence of protein spikes projecting above these lipid microdomains in p14-containing bilayers indicated that p14 associates with what are presumably liquid-ordered microdomains under aqueous conditions.

Although detergent-based analysis indicated that approximately half of the p14 present in transfected cells was not isolated in association with DRMs (Fig. 2*C*), the AFM results indicated that, when p14 resides in a lipid bilayer that contains liquid-ordered lipid microdomains, it has a high affinity for association with such microdomains. The under-representation of p14 association with lipid microdomains following detergent extraction may reflect either partial detergent extraction from lipid microdomains or trafficking of p14 through the endoplasmic reticulum-Golgi pathway (4), resulting in the presence of p14 in cell membranes generally considered to be deficient in microdomains (*i.e.* the endoplasmic reticulum). In any event, the AFM results clearly demonstrated that association of p14 with lipid microdomains does not depend on detergent-induced protein-lipid interactions.

Further detergent-based analysis provided insights into the heterogeneity of p14 association with cell membrane microdomains. Cell fractionation studies revealed that a significant proportion of p14 resides in detergent-resistant membrane environments, a typical feature of microdomain-associated proteins. Recent evidence suggests that DRMs may not capture intact microdomains, but may be composed of the lipid and/or protein components extracted from a heterogeneous population of distinct membrane microdomains that share certain detergent solubility properties (43, 54, 60, 64). Our biochemical and morphological studies support the concept of heterogeneous membrane microdomains that can be differentially extracted by select detergents into DRMs containing overlapping subsets of microdomains and that p14 associates with different subsets of these membrane microdomains. First, chromatographic results indicated that Triton X-100- and Lubrol WX-resistant membranes extracted from quail fibroblasts were composed of different lipid compositions, with LRMs relatively more enriched in cholesterol and containing less phosphatidylcholine compared with TRMs (Fig. 5). Similar results have been reported for other cell types, although detergent- and cell type-dependent influences on the nature of the isolated DRMs contribute to differences in the exact lipid formulations of the DRMs (43, 46). Regardless of the actual lipid composition of different DRMs, the fact that p14 was isolated in association with two distinct DRM populations indicates that p14 can associate with different lipid environments. This observation was consistent with our previous demonstration that purified p14 is functional in liposomes composed of different lipid formulations (11).

Second, although PLAP and p14 displayed the same detergent solubility properties and sensitivity to cholesterol depletion (Fig. 6), antibody-based co-patching and immunostaining of both proteins in intact plasma membranes revealed that p14 did not co-cluster with classical lipid-anchored raft markers (Fig. 7). These results are in accord with the view that plasma membranes contain distinct membrane microdomains and/or that these microdomains are highly dynamic structures. Furthermore, although different microdomains may share similar detergent solubility properties, these results further caution against directly equating the biochemical and biophysical properties of DRMs with the actual features of membrane microdomains present in intact cell membranes. As noted by others (21–23, 60), detergent extraction is likely to promote partial disruption and/or exchange between different membrane microdomains, making the presence of proteins in the same DRM fraction a poor prognosticator of their co-localization in native membranes.

The segregation of certain proteins into DRMs obtained using different detergents suggests that some microdomains can be subclassified based on their detergent solubility properties. Such is the case for proteins such as the microvillar protein prominin-1, the ATP cassette-binding transporter ABCA1, the small GTPase CDC42, and mature components of the γ-secre-

tase complex, all of which selectively associate in specific cell types with LRMs, but not TRMs (44–46). Proteins present in other microdomains escape subclassification based on differential detergent solubility because, as with p14, they are isolated in association with both LRMs and TRMs (45, 46, 55). However, cholesterol depletion helped to identify a subset of microdomain-associated p14 operationally defined by its cholesterol-dependent resistance to Lubrol WX extraction, providing a third line of evidence that p14 associates with different subsets of membrane microdomains. Cholesterol depletion resulted in a 50% displacement of p14 from LRMs (Fig. 6) and a coincident 80% inhibition of p14-induced syncytium formation, effects that were largely reversed by repletion of membrane cholesterol (Fig. 1). In contrast, cholesterol depletion had no significant effect on the association of p14 or PLAP with TRMs. The differential effects of cholesterol depletion on p14 association with DRMs also correlated with the increased cholesterol content of the LRMs *versus* TRMs (Fig. 5). We suggest that LRMs may capture a subpopulation of cholesterol-dependent microdomains not represented in the Triton X-100-resistant membrane fraction. Moreover, the effects of cholesterol depletion on p14-induced syncytium formation further suggested that the collection of compositionally distinct microdomains recovered following Lubrol WX extraction might contain a subpopulation of membrane microdomain-associated p14 more likely to be involved in the cell-cell fusion process.

Insights into the nature of the FAST proteins and the possible roles of microdomain populations present in LRMs provide a potential explanation for the role of Lubrol WX-resistant, p14-containing microdomains in the mechanism of p14-induced cell fusion. Microdomain-associated proteins extracted into LRMs have been implicated in regulating protein trafficking to, or the formation of, plasma membrane protrusions. For example, prominin-1 (CD133) is a pentaspan membrane protein that selectively localizes to microvilli or plasma membrane protrusions and that associates exclusively with LRMs, leading to the proposal that some Lubrol WX-resistant microdomains regulate protein localization to microvilli (45). Similarly, ABCA1 and CDC42 are both involved in filopodial formation and both associate with LRMs, suggesting that Lubrol WX-resistant microdomains may be involved in coordinating the formation of membrane protrusions (46, 65, 66). Based on the above considerations, it is plausible that p14 may use a subset of membrane microdomains, defined by their cholesterol-dependent resistance to Lubrol WX extraction, to localize a percentage of p14 to regions of the plasma membrane involved in close cell-cell contact. In addition to promoting cell-cell contact, such protrusions are likely to exhibit curvature stress and altered lipid packing. The altered biophysical properties of membranes in constrained protruding regions of the plasma membrane (33) may well contribute to lowered energy barriers for membrane fusion that can be circumvented by the FAST proteins, without the need for extensive energy input derived from structural rearrangements of complex metastable ectodomains. We are currently exploring these and other possible implications of p14 association with distinct subsets of membrane microdomains in the mechanism of p14-induced cell fusion.

Acknowledgments—We thank Jingyun Shou for expert technical assistance and Neale Ridgway for assistance with the N-BP-2 cell studies.

REFERENCES

1. Jahn, R., Lang, T., and Sudhof, T. C. (2003) *Cell* **112,** 519–533
2. Blumenthal, R., Clague, M. J., Durell, S. R., and Epand, R. M. (2003) *Chem. Rev.* **103,** 53–69
3. Shmulevitz, M., and Duncan, R. (2000) *EMBO J.* **19,** 902–912
4. Corcoran, J. A., and Duncan, R. (2004) *J. Virol.* **78,** 4342–4351
5. Dawe, S., and Duncan, R. (2002) *J. Virol.* **76,** 2131–2140
6. Duncan, R., Corcoran, J., Shou, J., and Stoltz, D. (2004) *Virology* **319,** 131–140
7. Earp, L. J., Delos, S. E., Park, H. E., and White, J. M. (2005) *Curr. Top. Microbiol. Immunol.* **285,** 25–66
8. Shmulevitz, M., Epand, R. F., Epand, R. M., and Duncan, R. (2004) *J. Virol.* **78,** 2808–2818
9. Corcoran, J. A., Syvitski, R., Top, D., Epand, R. M., Epand, R. F., Jakeman, D., and Duncan, R. (2004) *J. Biol. Chem.* **279,** 51386–51394
10. Dawe, S., Corcoran, J. A., Clancy, E. K., Salsman, J., and Duncan, R. (2005) *J. Virol.* **79,** 6216–6226
11. Top, D., de Antueno, R., Salsman, J., Corcoran, J. A., Mader, J., Hoskin, D., Touhami, A., Jericho, M. H., and Duncan, R. (2005) *EMBO J.* **24,** 2980–2988
12. Kozlov, M. M., and Chernomordik, L. V. (1998) *Biophys. J.* **75,** 1384–1396
13. Cohen, F. S., and Melikyan, G. B. (2004) *J. Membr. Biol.* **199,** 1–14
14. Bentz, J. (2000) *Biophys. J.* **78,** 886–900
15. Markosyan, R. M., Bates, P., Cohen, F. S., and Melikyan, G. B. (2004) *Biophys. J.* **87,** 3291–3298
16. Shmulevitz, M., Salsman, J., and Duncan, R. (2003) *J. Virol.* **77,** 9769–9779
17. Chernomordik, L. (1996) *Chem. Phys. Lipids* **81,** 203–213
18. Simons, K., and Ikonen, E. (1997) *Nature* **387,** 569–572
19. Edidin, M. (2003) *Annu. Rev. Biophys. Biomol. Struct.* **32,** 257–283
20. Brown, D. A., and London, E. (1998) *Annu. Rev. Cell Dev. Biol.* **14,** 111–136
21. Heerklotz, H. (2002) *Biophys. J.* **83,** 2693–2701
22. Lichtenberg, D., Goni, F. M., and Heerklotz, H. (2005) *Trends Biochem. Sci.* **30,** 430–436
23. Munro, S. (2003) *Cell* **115,** 377–388
24. Kenworthy, A. K., Nichols, B. J., Remmert, C. L., Hendrix, G. M., Kumar, M., Zimmerberg, J., and Lippincott-Schwartz, J. (2004) *J. Cell Biol.* **165,** 735–746
25. Simons, K., and Toomre, D. (2000) *Nat. Rev. Mol. Cell Biol.* **1,** 31–39
26. Chazal, N., and Gerlier, D. (2003) *Microbiol. Mol. Biol. Rev.* **67,** 226–237
27. Bavari, S., Bosio, C. M., Wiegand, E., Ruthel, G., Will, A. B., Geisbert, T. W., Hevey, M., Schmaljohn, C., Schmaljohn, A., and Aman, M. J. (2002) *J. Exp. Med.* **195,** 593–602
28. Nguyen, D. H., and Hildreth, J. E. (2000) *J. Virol.* **74,** 3264–3272
29. Scheiffele, P., Rietveld, A., Wilk, T., and Simons, K. (1999) *J. Biol. Chem.* **274,** 2038–2044
30. Kozak, S. L., Heard, J. M., and Kabat, D. (2002) *J. Virol.* **76,** 1802–1815
31. Takeda, M., Leser, G. P., Russell, C. J., and Lamb, R. A. (2003) *Proc. Natl. Acad. Sci. U. S. A.* **100,** 14610–14617
32. Fratti, R. A., Jun, Y., Merz, A. J., Margolis, N., and Wickner, W. (2004) *J. Cell Biol.* **167,** 1087–1098
33. Huttner, W. B., and Zimmerberg, J. (2001) *Curr. Opin. Cell Biol.* **13,** 478–484
34. Liao, Z., Graham, D. R., and Hildreth, J. E. (2003) *AIDS Res. Hum. Retroviruses* **19,** 675–687
35. Pai, J. T., Guryev, O., Brown, M. S., and Goldstein, J. L. (1998) *J. Biol. Chem.* **273,** 26138–26148
36. Ridgway, N. D., and Lagace, T. A. (2003) *Biochem. J.* **372,** 811–819
37. Harder, T., Scheiffele, P., Verkade, P., and Simons, K. (1998) *J. Cell Biol.* **141,** 929–942
38. Folch, J., Lees, M., and Sloane Stanley, G. H. (1957) *J. Biol. Chem.* **226,** 497–509
39. de Antueno, R. J., Elliot, M., and Horrobin, D. F. (1994) *Lipids* **29,** 327–331

40. Kielian, M., Chatterjee, P. K., Gibbons, D. L., and Lu, Y. E. (2000) *Subcell. Biochem.* **34,** 409–455
41. Melkonian, K. A., Ostermeyer, A. G., Chen, J. Z., Roth, M. G., and Brown, D. A. (1999) *J. Biol. Chem.* **274,** 3910–3917
42. Kunimoto, M., Shibata, K., and Miura, T. (1989) *J. Biochem.* (*Tokyo*) **105,** 190–195
43. Schuck, S., Honsho, M., Ekroos, K., Shevchenko, A., and Simons, K. (2003) *Proc. Natl. Acad. Sci. U. S. A.* **100,** 5795–5800
44. Vetrivel, K. S., Cheng, H., Lin, W., Sakurai, T., Li, T., Nukina, N., Wong, P. C., Xu, H., and Thinakaran, G. (2004) *J. Biol. Chem.* **279,** 44945–44954
45. Roper, K., Corbeil, D., and Huttner, W. B. (2000) *Nat. Cell Biol.* **2,** 582–592
46. Drobnik, W., Borsukova, H., Bottcher, A., Pfeiffer, A., Liebisch, G., Schutz, G. J., Schindler, H., and Schmitz, G. (2002) *Traffic* **3,** 268–278
47. Shogomori, H., and Brown, D. A. (2003) *Biol. Chem.* **384,** 1259–1263
48. Reviakine, I., and Brisson, A. (2000) *Langmuir* **16,** 1806–1815
49. Saslowsky, D. E., Lawrence, J., Ren, X., Brown, D. A., Henderson, R. M., and Edwardson, J. M. (2002) *J. Biol. Chem.* **277,** 26966–26970
50. Lawrence, J. C., Saslowsky, D. E., Edwardson, J. M., and Henderson, R. M. (2003) *Biophys. J.* **84,** 1827–1832
51. Nicolini, C., Baranski, J., Schlummer, S., Palomo, J., Lumbierres-Burgues, M., Kahms, M., Kuhlmann, J., Sanchez, S., Gratton, E., Waldmann, H., and Winter, R. (2006) *J. Am. Chem. Soc.* **128,** 192–201
52. Henderson, R. M., Edwardson, J. M., Geisse, N. A., and Saslowsky, D. E. (2004) *News Physiol. Sci.* **19,** 39–43
53. van Duyl, B. Y., Ganchev, D., Chupin, V., de Kruijff, B., and Killian, J. A. (2003) *FEBS Lett.* **547,** 101–106
54. Brugger, B., Graham, C., Leibrecht, I., Mombelli, E., Jen, A., Wieland, F., and Morris, R. (2004) *J. Biol. Chem.* **279,** 7530–7536
55. Slimane, T. A., Trugnan, G., van IJzendoorn, S. C. D., and Hoekstra, D. (2003) *Mol. Biol. Cell* **14,** 611–624
56. Hansen, G. H., Immerdal, L., Thorsen, E., Niels-Christiansen, L. L., Nystrom, B. T., Demant, E. J., and Danielsen, E. M. (2001) *J. Biol. Chem.* **276,** 32338–32344
57. Hao, M., Mukherjee, S., and Maxfield, F. R. (2001) *Proc. Natl. Acad. Sci. U. S. A.* **98,** 13072–13077
58. Schroeder, R. J., Ahmed, S. N., Zhu, Y., London, E., and Brown, D. A. (1998) *J. Biol. Chem.* **273,** 1150–1157
59. Vyas, K. A., Patel, H. V., Vyas, A. A., and Schnaar, R. L. (2001) *Biol. Chem.* **382,** 241–250
60. Wilson, B. S., Steinberg, S. L., Liederman, K., Pfeiffer, J. R., Surviladze, Z., Zhang, J., Samelson, L. E., Yang, L. H., Kotula, P. G., and Oliver, J. M. (2004) *Mol. Biol. Cell* **15,** 2580–2592
61. Cleverley, D. Z., Geller, H. M., and Lenard, J. (1997) *Exp. Cell Res.* **233,** 288–296
62. Rinia, H. A., Snel, M. M., van der Eerden, J. P., and de Kruijff, B. (2001) *FEBS Lett.* **501,** 92–96
63. Saslowsky, D. E., Lawrence, J. C., Henderson, R. M., and Edwardson, J. M. (2003) *J. Membr. Biol.* **194,** 153–164
64. Vetrivel, K. S., Cheng, H., Kim, S. H., Chen, Y., Barnes, N. Y., Parent, A. T., Sisodia, S. S., and Thinakaran, G. (2005) *J. Biol. Chem.* **280,** 25892–25900
65. Tsukamoto, K., Hirano, K., Tsujii, K., Ikegami, C., Zhongyan, Z., Nishida, Y., Ohama, T., Matsuura, F., Yamashita, S., and Matsuzawa, Y. (2001) *Biochem. Biophys. Res. Commun.* **287,** 757–765
66. Bared, S. M., Buechler, C., Boettcher, A., Dayoub, R., Sigruener, A., Grandl, M., Rudolph, C., Dada, A., and Schmitz, G. (2004) *Mol. Biol. Cell* **15,** 5399–5407

The p14 Fusion-associated Small Transmembrane (FAST) Protein Effects Membrane Fusion from a Subset of Membrane Microdomains

Jennifer A. Corcoran, Jayme Salsman, Roberto de Antueno, Ahmed Touhami, Manfred H. Jericho, Eileen K. Clancy and Roy Duncan

J. Biol. Chem. 2006, 281:31778-31789.
doi: 10.1074/jbc.M602566200 originally published online August 26, 2006
